

M. PAWŁOWSKI^{1,2}, P. KAMIŃSKI¹, R. KOZŁOWSKI¹, S. JANKOWSKI³,
M. WIERZBOWSKI²

¹Institute of Electronic Materials Technology, 01-919 Warsaw, Poland

²Military University of Technology, 00-908 Warsaw 49, PO Box 50, Poland

³Warsaw University of Technology, 00-665 Warsaw, Poland

e-mail: mpawlowski@itme.edu.pl

INTELLIGENT MEASURING SYSTEM FOR CHARACTERISATION OF DEFECT CENTRES IN SEMI-INSULATING MATERIALS BY PHOTOINDUCED TRANSIENT SPECTROSCOPY

An intelligent measurement system for the characterisation of defect centres in semi-insulating materials is presented. The system utilises two-dimensional analysis of the photocurrent transients digitally recorded in a broad range of temperatures. The spectral analysis is carried out by two independent methods: the two-dimensional correlation procedure and the procedure based on the inverse Laplace transformation algorithm. Parameters of a defect centre are determined using the neural network algorithm which is based on two hidden neurons in the form of two-dimensional sigmoid functions used to obtain a morphological match of the approximating function to the shape of the fold on the spectral surface. The system is shown to be a powerful tool for studies of defect structure of high-resistivity semiconductors.

Keywords: Photoinduced Transient Spectroscopy (PITS), neural network, computational intelligence, defect centres, semi-insulating materials

1. INTRODUCTION

High-resistivity semiconductors are very important materials in terms of application in various fields of advanced electronics and optoelectronics. Semi-insulating (SI) GaAs and InP wafers are key elements of high-speed devices and integrated circuits. In particular, SI InP is an important material in terms of manufacturing high-frequency devices and optoelectronic integrated circuits (OEICs) for high-speed telecommunication and computer networks. The SI InP crystals are usually grown by the liquid-encapsulated Czochralski (LEC) method and their properties are mainly controlled by point defects introduced during crystallisation. These defects result in the perturbation of the local lattice potential and creation of either shallow or deep bound electron states in the band gap. So far, a high resistivity of InP ranging from 10^7 to 10^9 Ωcm has been mainly achieved by doping with iron which acts as a deep acceptor compensating residual shallow donors resulting from contamination with silicon and sulphur atoms [1]. Doping with Fe is mainly performed during the crystal growth, however, the attempts have been made to obtain SI InP by shaping the defect structure of high-purity wafers through annealing under a high phosphorus vapour pressure or through iron diffusion [2, 3]. High-resistivity silicon wafers are widely used for fabrication of particle detectors. The understanding of changes in defect structure of silicon lattice induced by irradiation is of great importance in terms of manufacturing devices operating in radiation environments. Further development of radiation-resistant solar cells for Space applications, as well as particle detectors for high-energy physics experiments, requires deeper knowledge of the properties and generation mechanisms of irradiation-induced point defects.

Defect levels in the semiconductor bandgap have significant effect on device performance. They can act as trapping centres by capturing majority or minority carriers as well as recombination centres while capturing both types of carriers. In low resistivity materials, capture and emission of carriers at defect levels is usually characterised by deep level

transient spectroscopy (DLTS) [4]. However, for high resistivity materials, the conventional capacitance-mode DLTS technique is not applicable due to the difficulty of filling the levels by a change in electrical bias. Defect centres in semi-insulating materials have been mostly characterized by thermally stimulated current (TSC) and photoinduced transient spectroscopy (PITS) measurements [3, 5-8]. The main disadvantage of the former method is poor resolution since the centres are filled with charge carriers at a temperature much lower than that of thermal emission. Moreover, the results are strongly dependent on the sample illumination conditions, which gives rise to some ambiguous peaks [3, 5]. The PITS technique, also referred to as photo-induced current transient spectroscopy (PICTS), is free of these deficiencies. This technique relies on filling the levels with carriers generated by optical pulse and analyzing the photocurrent decay observed after switching the light off as a function of temperature. Since its development by Hurtes *et al.* in 1978 [9], photoinduced transient spectroscopy had been firstly used as an analogue technique. In order to evaluate the thermal emission rate of trapped charge carriers, the photocurrent decay was analysed as a function of temperature using analogue equipment, usually a double-gated boxcar integrator, similarly as in conventional capacitance-mode deep level transient spectroscopy (DLTS) [4]. Recently digital recording of the photocurrent decays has been implemented, and the analysis is based on the assumption that the photocurrent decay is given by a single-exponential expression, the time constant of which is equal to the reciprocal of the thermal emission rate [10, 11]. Application of digital technique to recording of the photocurrent transients simplifies and fastens the characterisation process [12]. The photocurrent transients are recorded in a wide range of temperatures during one temperature scan. Then the set of recorded data can be analysed by means of a digital correlation procedure similar to the previous analogue one. In many cases, however, this assumption is not valid, for at some temperatures the photocurrent decay may result from the thermal emission of charge carriers from two or more defect centres [13]. The calculation process of the defect parameters usually comprises two stages. First the one-dimensional PITS spectra for various emission rate windows are obtained. Next, temperatures corresponding to the position of the peaks are estimated by best-fitting spectra with the Gaussian function and the temperature dependence of the thermal emission rate is determined. The parameters of the deep traps are calculated using the Arrhenius plot [14]. So, the calculation procedure is very time consuming.

In this paper a new approach to extraction of trap parameters from digitally recorded photocurrent transients at various temperatures is presented. The approach is based on treatment of the transients as a function of two variables, time and temperature. Using the correlation procedure or inverse Laplace transform algorithm the experimental data are transformed into spectral surface in co-ordinates of temperature and emission rate. The processes of the thermal emission charge carriers from deep traps manifest themselves as the folds on the spectral surface. Each fold is best-fitted separately using a two-dimensional numerical model. The trap parameters are obtained as the parameters of the approximating function from the best fit of the model to the fold using computational intelligence methods [15]. This approach overcomes the drawback of the conventional procedure in which the experimental data are analysed step-by-step by means of a set of one-dimensional spectra determined for various emission rate windows. The two-dimensional spectrum automatically gives the temperature dependence of the emission rate determined by the ridgeline of the fold on spectral surface. In other words, it enables the defect signature to be obtained as a result of one calculation process. The new approach has been implemented in the intelligent experimental system for characterisation of defect centres in semi-insulating materials. In this system the computational intelligence is used for determination of the parameters of defect centres on the grounds of the spectral fringes obtained as a result of the two-dimensional correlation procedure and inverse Laplace transform.

2. ALGORITHMS OF TWO-DIMENSIONAL ANALYSIS OF PHOTOCURRENT DECAYS

2.1 Correlation procedure

The mathematical model that is usually assumed to describe the photocurrent decay after switching off the illumination pulse has the form [16]:

$$i(t, T_j) = \sum_{p=1}^P I_p(T_j) \exp[-e_{Tp}(T_j)t], \quad (1)$$

where P is the number of exponential components, I_p is the amplitude of the p -th component, T_j is the sample temperature for j -th measurement and e_{Tp} is the thermal emission rate for electrons from the p -th trap. The temperature dependence of the emission rate for electrons is given by the well-known Arrhenius formula

$$e_{Tp}(T_j) = A_p T_j^2 \exp(-E_{Tp}/k_B T_j), \quad (2)$$

where E_{Tp} is the p -th trap activation energy, k_B is the Boltzmann constant and $A_p = \sigma_p \gamma$ is the product of the trap capture cross-section σ_p and a material constant γ .

The experimental data are in the form of a set of photocurrent transients $i(t, T_j)$ digitally recorded for J values of temperature in a given temperature range $[T_1, T_2]$ with a step ΔT . At first, the transients are converted into the set of one-dimensional spectra $S_{Cg}(T)$ for g values of emission rate e_{Tg} using the correlation procedure given by

$$S_{Cg}(T) = B \int_0^{t_N} i(t, T) w_g(t, e_{Tg}) dt, \quad (3)$$

where $w_g(t, e_{Tg})$ is the weighting function for the value e_{Tg} of the emission rate, t_N is the width of the transient and B is a normalisation constant. The weighting function can be of various forms. It can be an exponential, sinusoidal or rectangular waveform, as well as in the shape of several pulses with various amplitudes [17]. Usually the simplest form of the weighting function is chosen

$$w_g(t, e_{Tg}) = \delta[t - t_1(e_{Tg})] - \delta[t - t_2(e_{Tg})], \quad (4)$$

where δ denotes Dirac's delta function and t_1 and t_2 determine the shift of δ -function along the time axis. Each spectrum $S_{Cg}(T)$ is calculated for the given emission rate window determined by the time points t_1 and t_2 . The emission rate window indicated by the spectrum maximum at the temperature T_{MAX} [18] is calculated from the condition $dS_C/dT = (dS_C/de_T)(de_T/dT) = 0$. For typical value of the ratio $t_2/t_1 = 3$ the following relations $t_1 = 1.23/e_{Tg}$ and $t_2 = 3.69/e_{Tg}$ between the time points and the emission rate are obtained. Next, the experimental spectral surface $S_C(T, e_T)$ is formed by collecting the one-dimensional spectra $S_{Cg}(T)$ for g values of emission rate in the form of the spatial graph. So, the occurrence of the thermal emission from a defect centre manifests itself by the fold on the surface $S_C(T, e_T)$ with the ridgeline showing the temperature dependence of the emission rate. In order to extract the parameters of the

defect centre, the part of the spectral surface $S_C(T, e_T)$ with one fold is selected and approximated with a two-dimensional function.

2.2 Inverse Laplace transformation algorithm

The photocurrent decay $i(t, T_j)$ observed at the temperature T_j after switching of the illumination pulse can be described by means of the expression containing the Fredholm integral of the first kind [19]:

$$i(t, T_j) = \int_0^{\infty} S_{Lj}(e_T) \exp(-e_T t) de_T, \quad (5)$$

where $S_{Lj}(e_T)$ is the spectral density function. When the kernel is given by an exponential function, the Fredholm integral is in the form of the Laplace transform and the problem relies on determination of the spectral density function $S_{Lj}(e_T)$ using suitable numerical algorithms [20-22]. So, in order to solve this problem it is necessary to perform an inverse Laplace transformation and find such a form of the function $S_{Lj}(e_T)$ that will be a solution of the integral Eq. (5). For the ideal $i(t, T_j)$ waveform composed of several exponential components, the solution of Eq. (5) is unambiguous. In reality, however, the photocurrent decay $i(t, T_j)$ contains noise component and the reference level is unknown. Therefore, the number of solutions can be large and the solutions can be much different.

Because of the discrete form of data producing the photocurrent decay in the numerical calculations the integral in equation (5) is replaced by the sum:

$$i(t, T_j) = \sum_{m=1}^M S_{Lj}(e_{Tm}) \exp(-e_{Tm} t), \quad (6)$$

where M is the number of points in the set of emission rate values e_T with the limits $e_{T1} = e_{Tmin}$ and $e_{TM} = e_{Tmax}$. The numerical procedure can be written in the matrix form:

$$i_j = K S_{Lj}, \quad (7)$$

where $i_j = (i_1, i_2, \dots, i_N)_j$ is the column vector of N elements of discrete data describing the waveform of the photocurrent decay, $S_{Lj} = (s_{L1}, s_{L2}, \dots, s_{LM})_j$ is the column vector of M values of the spectral density function and K is the matrix of the elements $\alpha_{mn} = \exp(-e_{Tm} t_n)$ with dimensions $N \times M$, representing the integral Laplace operator:

$$\mathbf{K} = \begin{bmatrix} \alpha_{11} & \alpha_{21} & \cdots & \alpha_{M1} \\ \alpha_{12} & \alpha_{22} & \cdots & \alpha_{M2} \\ \vdots & \vdots & \ddots & \vdots \\ \alpha_{1N} & \alpha_{2N} & \cdots & \alpha_{MN} \end{bmatrix}. \quad (8)$$

A numerical procedure allowing for obtaining the solution S_{Lj} is based on the Tikhonov regularisation [21, 22]. The spectral analysis of the photocurrent decays is practically carried out by means of the CONTIN computer program developed and realised by S.W. Provencher [22, 23]. The two-dimensional Laplace spectrum $S_L(e_T, T)$ in co-ordinates: emission rate, temperature is formed by putting together many one-dimensional spectra $S_{Lj}(e_T)$ received as

result of transformation of the photocurrent decays recorded at J different temperatures. The sharp folds occurring in the spectral surface are related to the thermal emission of charge carriers from defect centres. These folds are visualised as the spectral fringes obtained by the projection of the folds on the plane determined by co-ordinates (e_T, T) . The projections of the ridgelines of the folds on this plane give the temperature dependences of emission rates for defect centres described by the Arrhenius equation.

2.3 Neural network approximation

In order to determine the parameters of defect centres, the folds occurring in the two-dimensional spectra in the domain of the temperature and emission rate, obtained using both the correlation procedure (COP) and the inverse Laplace transform algorithm (ILT), are approximated with a continuous function represented by a neural network (NN) [24]. The neural approximator has the form of two-layered perceptron whose inputs are the arguments of the spectral surface. The activation function of hidden neurons is assumed as a weighted sum of two-sigmoid functions. Hence, each hidden neuron can model the lateral surface of the two-dimensional spectrum. When added together, they create the fold that matches the experimental fold corresponding to a specific defect centre. The parameters of this centre, such as activation energy and apparent capture cross section, are directly obtained as the weight coefficients of hidden neurons by means of a certain optimization process.

Our goal is to find two parameters of a line which is the projection of the ridgeline of the p -th spectral fold on the 2-dimensional Arrhenius plane in co-ordinates $x = 1000/T$ and $y = \ln(T^2/e_T)$. So, the Arrhenius formula can be written as a line equation $y = a \cdot x + b$, where $a = E_{Tp}/(1000 \cdot k_B)$ and $b = -\ln(A_p)$. To achieve the goal we use a neural network as a universal approximator, which can approximate any function with the desired accuracy upon a set of measurement points. The NN we use has a special structure, which enables us to obtain the line parameters directly from NN parameters. A neural network is represented by the following formula:

$$Z(x, y, \mathbf{w}) = w_5 h_1 + w_6 h_2 + b_3, \quad (9)$$

where x and y are arguments of the function and are called inputs to the NN, $h_1 = \tanh(w_1 x + w_2 y + b_1)$ and $h_2 = \tanh(w_3 x + w_4 y + b_2)$ are the outputs of hidden neurons, $Z(x, y, \mathbf{w})$ is the output of the NN and $\mathbf{w} = \{w_1, w_2, w_3, w_4, w_5, w_6, b_1, b_2, b_3\}$ is a vector of parameters, called *weights*, determining the output of the NN. Each hidden neuron h_i represents one of the two lateral surfaces of the approximating fold. The sum of the lateral surfaces represented by the both hidden neurons gives the final fold at the Z output of the NN. The shape of this surface, i.e. direction, position and slope, is controlled by the parameters w_1 , w_2 and b_1 of the hidden neuron h_1 , as well as by the parameters w_3 , w_4 , and b_2 of the hidden neuron h_2 . The height of the fold is determined by the parameters w_5 and w_6 . The aim of this approach is to approximate the p -th spectral fold, formed by the R data points $(T_r, e_{Tr}, S_r)_p$, with the continuous NN fold function Z in the co-ordinates $1000/T$ and $\ln(T^2/e_T)$. To achieve this, it is necessary to find the vector \mathbf{w} which minimises the error between the data points and the output of NN. The error is defined as

$$\varepsilon = \frac{1}{2} \sum_{r=1}^R \left\{ S_r \left[\frac{1000}{T_r}, \ln \frac{(T_r)^2}{e_{Tr}} \right] - Z \left[\frac{1000}{T_r}, \ln \frac{(T_r)^2}{e_{Tr}} \right], \mathbf{w} \right\}^2, \quad (10)$$

where $S_r[(1000/T_r), \ln(T_r^2/e_{Tr})]$ is the value of the spectral surface for temperature T_r and emission rate e_{Tr} and r is a number of a data point from a set of all approximated data points R . The optimisation (learning of the NN) is performed using both back propagation and the Levenberg-Marquardt algorithm [25]. As a result of the optimisation process, we obtain the vector w which gives us the parameters $a_{h1} = w_1/w_2$, $b_{h1} = w_1/b_1$ for h_1 and $a_{h2} = w_3/w_4$, $b_{h2} = w_3/b_2$ for h_2 . To find the slope a of the line $y = ax + b$ we take the mean value of the two slopes expressed as $a = \tan(0.5(\alpha_{h1} + \alpha_{h2}))$, where $\alpha_{h1} = \arctan(a_{h1})$ and $\alpha_{h2} = \arctan(a_{h2})$. In order to find the value of b first we seek a cross point (x_0, y_0) of the two lines $y_1 = a_{h1}x + b_{h1}$ and $y_2 = a_{h2}x + b_{h2}$. Upon the co-ordinates of the cross point (x_0, y_0) and direction a we calculate the value of b as $b = -ax_0 + y_0$. Having the a and b values, the parameters of the p -th defect centre E_{Tp} and A_p are given by the following expressions: $E_{Tp} = 8.62 \times 10^{-2} a$ and $A_p = \exp(-b)$.

3. INTELLIGENT MEASURING SYSTEM FOR STUDYING DEFECT CENTRES IN SEMI-INSULATING MATERIALS

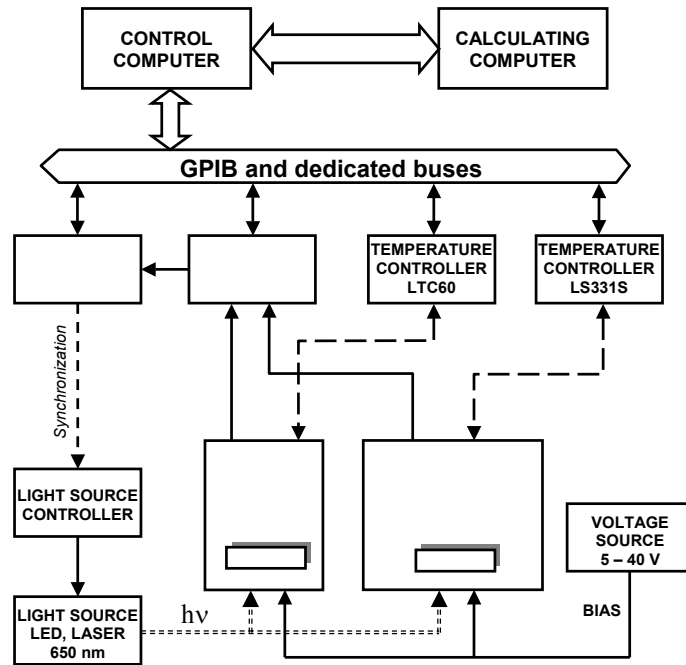


Fig. 1. Experimental setup to measure the photocurrent decays in a broad range of temperatures and to determine the temperature dependences of emission rate from defect centres.

Figure 1 shows the block diagram of the apparatus used for measuring photocurrent decays and determination of the temperature dependences of emission rate from detected defect centres. For the measurements, arrays of ohmic contact pairs are deposited on the polished surface of the semi-insulating material wafer. The gap between two electrodes is 0.7 mm. The wafers are cut into chips of $4 \times 9 \text{ mm}^2$ in area, which are mounted in the sample holder of a cryostat or high temperature vacuum head. The experiments are carried out in the temperature range 20-700 K. The excess carriers are generated in the region between the two electrodes by a 5-mW laser diode beam with the wavelength of 650 nm (photon energy 1.96 eV). A typical flux of excitation light was equal to $1.1 \times 10^{18} \text{ cm}^{-2} \text{ s}^{-1}$. The width of illumination pulses can be varied from 1 to 100 ms and the period between pulses ranges from 10 to 1000 ms. The voltage between two co-planar electrodes can change in a range of 5-40 V. The photocurrent transients are digitised with a 12-bit resolution and sampling frequency of 1 MHz. The

photocurrent decays are normalised with respect to the photocurrent amplitude at the end of the light pulse.

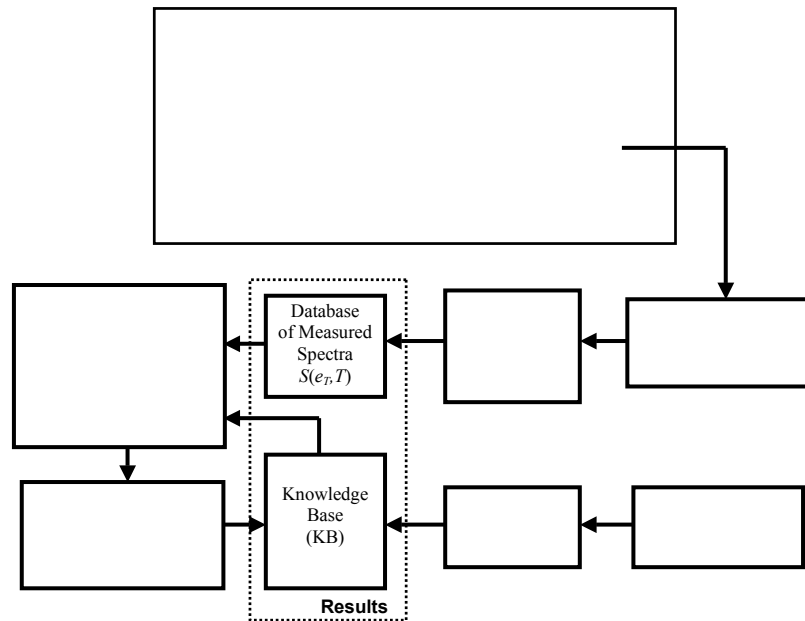


Fig. 2. Schematic illustration of the intelligent experimental system for characterisation of defect centres in semi-insulating materials.

The schematic illustration of the intelligent system for characterisation of defect centres in high-resistivity semiconductors is shown in Fig.2. The basic advantage of the system relies on the application of two dimensional analysis of the photocurrent decays and computational intelligence to extract the parameters of defect centres from the two-dimensional spectra in the domain of temperature and emission rate [15]. For the analysis, both the correlation procedure and inverse Laplace transformation algorithm are used [15, 19]. The advantage of the COP is a very small sensitivity to the noise component in the photocurrent decays. On the other hand, however, it gives a low resolution of defect centres with similar parameters. The ILT algorithm gives a very high resolution but it is very sensitive to the noise and may produce ambiguous results. So, the both methods of analysis are complementary and in our approach the COP is used for the verification of the results obtained by the ILT. In order to determine the parameters of defect centres the ridgelines of the COP spectra and the fringes of the ILT spectra are fitted with the Arrhenius equation [19] using a neural network (NN) [24]. For identification of each defect centre, the obtained parameters: activation energy E_T and pre-exponential factor A , are compared with the data in the knowledge base (KB), where the defect properties reported in the available publications are stored and catalogued. The set of actions performed by the system in order to determine the parameters of the defect centres (E_T, A) and to make a tentative identification of the centres is presented in Fig. 3. It is worth noting that there are two loops implemented in the procedure of extraction of defect centre parameters from the photocurrent decays. The first one serves the verification of the initial settings for running the CONTIN program and the second is used for verification of choosing the approximation region within the fold.

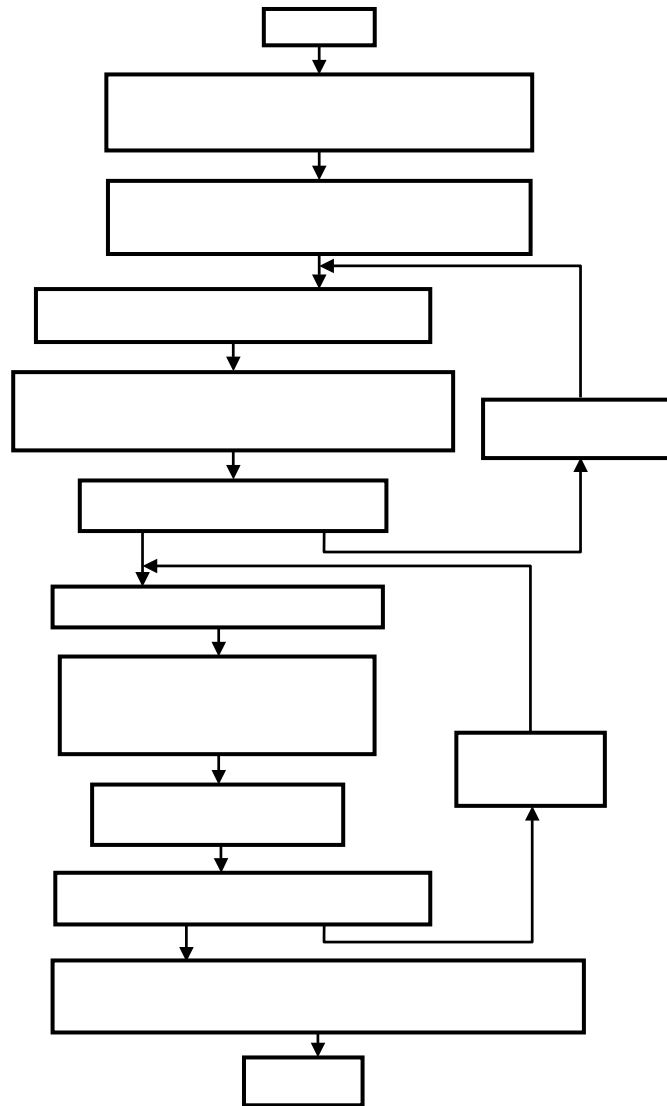


Fig. 3. The flow diagram of the procedure implemented in the intelligent system for the extraction of defect centres parameters.

4. APPLICATIONS OF THE INTELLIGENT MEASURING SYSTEM TO THE INVESTIGATION OF DEFECT CENTRES IN SEMI-INSULATING MATERIALS

Application of the intelligent measurement system to the investigation of defect centres in semi-insulating materials is exemplified by studying compensation centres in SI InP and radiation centres formed in epitaxial silicon by irradiation with high proton fluences.

4.1 Investigation of compensation centres in semi-insulating InP

The samples used for characterization of defect centres were prepared from the (100) wafers originated from two bulk InP single crystals grown by the LEC technique. The samples, labelled as #24asd, were prepared from the wafer produced from the as-grown semi-insulating iron-doped crystal. The samples, labelled as #33pje, came from the wafer produced from the undoped crystal with a resistivity of $2100 \Omega\text{cm}$ and annealed at 950°C for 40 h. The annealing was performed in sealed ampoules under a phosphorus vapour pressure of 1×10^5 Pa. The Fe concentration in the samples #24asd and #33pje was determined by the secondary

ion mass spectroscopy (SIMS) and glow discharge mass spectrometry (GDMS), respectively. The parameters of the both kinds of samples are summarized in Table 1. According to the data given in Table 1, the samples were chosen in order to compare the defect structure of crystals with significantly different iron concentrations and different values of the Hall mobility.

Table 1. Properties of the SI InP samples used for characterisation of defect centres

Sample properties	Sample #24asd	Sample #33pje
Resistivity at 300 K (Ωcm)	1.8×10^7	2.2×10^7
Resistivity at 100 K (Ωcm)	7.1×10^9	7.0×10^7
Hall mobility at 300 K (cm^2/Vs)	2638	4500
[Fe] (cm^{-3})	9.0×10^{15}	undoped, residual concentration 8.8×10^{14}
E_{TDDC}^* (eV)	0.63	0.43
Preparation conditions	as-grown	annealed at 950°C , 40 h, 1×10^5 Pa

* Activation energy determined from the temperature dependence of dark current

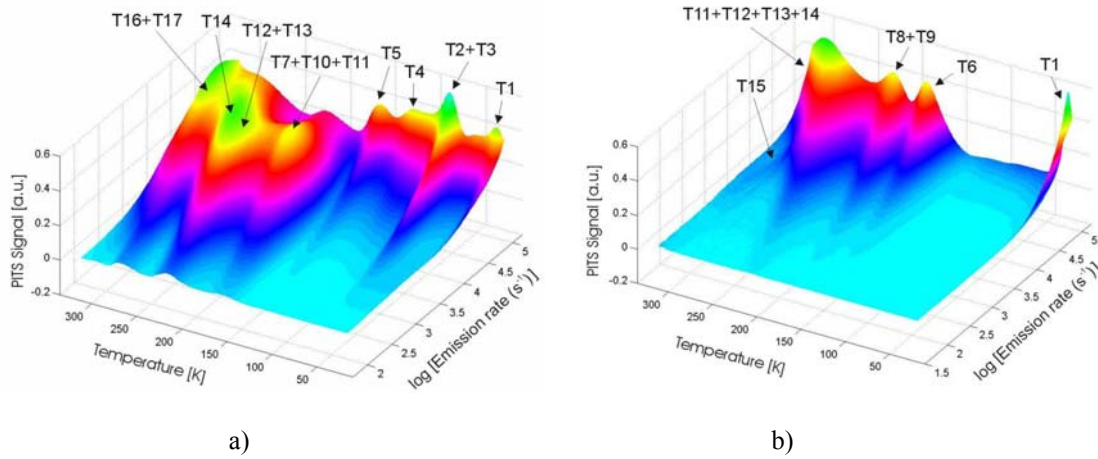
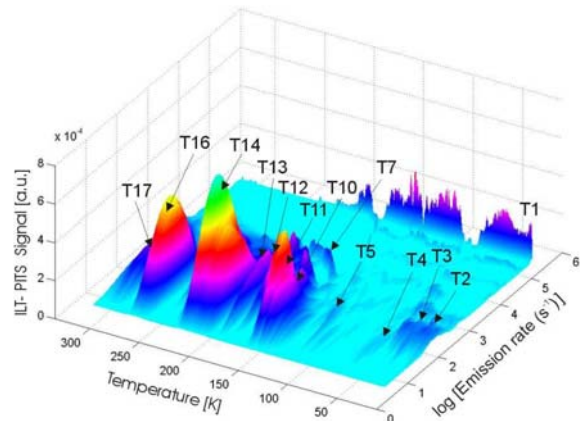
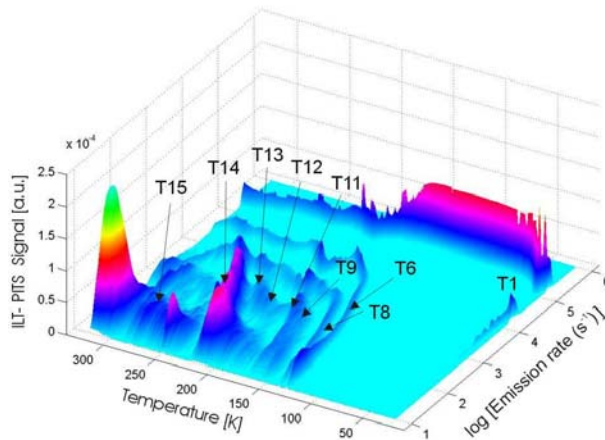


Fig.4. 3-D visualisation of the folds occurring on the correlation spectral surface for SI InP:Fe (a) and undoped SI InP (b) in the temperature range of 20-320 K and in the range of emission rate windows of 10^2 - 10^5 s^{-1} .

Figure 4 illustrates the comparison of the spectral surfaces for the SI InP:Fe (Fig. 4a) and for the undoped SI InP (Fig. 4b). It is seen that the defect structure of the former material is much complex than that of the latter. In particular, on the spectral surface for SI InP:Fe are observed the folds related to defect centres labelled as T2, T3, T4, T5 and T10. Moreover, there is also a broad fold resulting from the thermal emission of charge carriers from the deep centres T16 and T17.



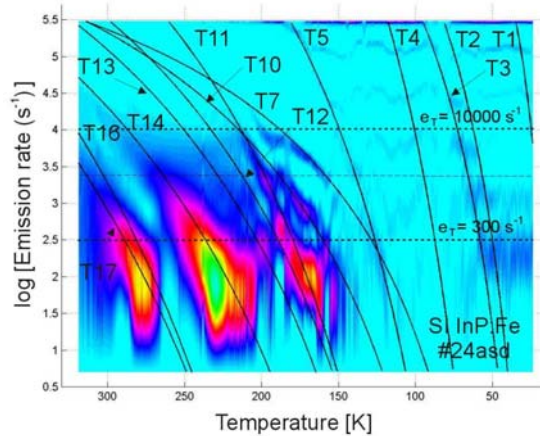
a)



b)

Fig. 5. 3-D visualisation of the folds occurring on the ILT spectral surface for SI InP:Fe (a) and undoped SI InP (b) in the temperature range of 20-320 K and in the range of emission rate windows of 10^2 - 10^5 s^{-1} .

Figure 5 shows the comparison of the spectral surfaces obtained for the both materials using the ILT algorithm. The better resolution of the ILT procedure manifests itself through the sharp, clearly distinguished ridgelines of the folds. The spectral fringes for defect centres detected in the both kinds of SI InP, obtained as a result of the projection of the folds in the spectral surfaces on the plane determined by the temperature and emission rate axes, are presented in Fig. 6.



a)

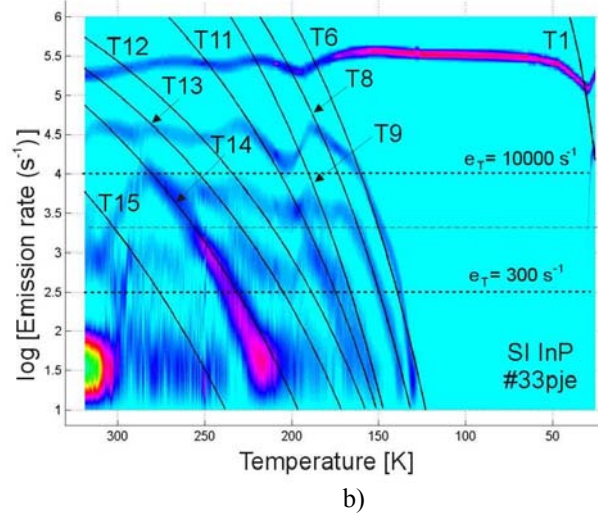


Fig. 6. Experimental spectral fringes for defect centres detected in SI InP:Fe (a) and undoped SI InP (b) obtained as a result of ILT procedure implemented to the analysis of the photocurrent decays. The solid lines illustrate the temperature dependences of the emission rate for detected defect centres determined by means of the neural network approximation.

Table 2. Summary of parameters of defect centres detected in SI InP using the intelligent measuring system.

Defect label	Activation energy E_T (meV)	Pre-exponential factor A ($s^{-1}K^{-2}$)	Tentative identification	Occurrence
T1	10	3.0×10^4	shallow donors: S, Si (e) [26, 27]	Fe-doped and undoped
T2	65	1.5×10^5	shallow donor: native defect or native defect - impurity complex [27-29]	Fe-doped
T3	75	3.0×10^5	$V_{In}H_4^+$ [30]	Fe-doped
T4	195	1.0×10^7	related to V_P [3] (e), P2 [5]	Fe-doped
T5	220	1.5×10^7	$P_{In}^{+/++}$ [2] (e), P3 [5], A1 [6]	Fe-doped
T6	290	9.5×10^7	$V_{In}H_2^+$ [30]	undoped
T7	95	1.0×10^2	$V_{In}^{+/0}$ [31] (h)	Fe-doped
T8	300	2.5×10^8	T1 [8], A2 [6]	undoped
T9	360	2.5×10^8	A3 [6], 0.37 eV [7], T_d [3]	undoped
T10	155	9.0×10^2	$V_{In}^{0/-}$ [31] (h)	Fe-doped
T11	305	2.5×10^6	E6 [32] (e), P6 [5]	Fe-doped and undoped
T12	255	1.0×10^4	related to Zn and Fe [33]	Fe-doped and undoped
T13	280	7.0×10^4	P5 [5]	Fe-doped and undoped
T14	350	1.5×10^5	Fe related [34]	Fe-doped and undoped
T15	470	9.0×10^7	A4 [6], T_b [3], E3 [32]	undoped
T16	640	2.0×10^9	$Fe^{2+/3+}$ [34] (e)	Fe-doped
T17	590	4.0×10^7	complex involving Fe^{2+} ; B2 [35], E1 [32] (e)	Fe-doped

Comments: e and h denote electron and hole trap, respectively.

In order to determine the parameters of defect centres the ILT folds were approximated with a sigmoid function using the neural network algorithm. It is worth noting that the approximation region of each fold observed in fig. 6 (a) and fig. 6 (b) chosen as a result of the verification process of the fold selection (see fig. 3) was in the range of emission rate between 300 and 10000 s^{-1} . The shape of the spectral fringes observed in the range of emission rate below 300 s^{-1} is determined mainly by noise that masks thermal emission processes from deep

levels. On the other hand, in the range of emission rate above 10000 s^{-1} there are observed folds related to pulse response of current amplifier. As a result, the parameters of the Arrhenius equation: activation energy E_T and pre-exponential factor A were directly obtained as the weight coefficients of the hidden neurons [24]. For identification, the parameters of each defect centre were compared with the data in the knowledge base, where the defect properties reported in the available publications are stored and catalogued. The properties of the detected defect centres determined by means of the intelligent experimental system are summarized in Table 2. The results shown in Table 2 indicate that the defect structure of SI InP is very complex and the material properties are affected by a number of various point defects. In the both materials a shallow donor with activation energy of 10 meV is detected. This donor is present due to contamination of these materials either with sulphur or silicon. Moreover, in the as-grown Fe-doped InP, a centre with activation energy of 75 meV attributed to the donor complex $V_{\text{In}}\text{H}_4^+$ is found. The shallow donors in this material are compensated with Fe-related deep acceptors having activation energies of 590 and 640 meV. In the annealed InP, a centre assigned to the complex $V_{\text{In}}\text{H}^{2-}$ with activation energy of 290 meV is observed. This centre is formed as a result of the thermal decomposition of the hydrogen complex $V_{\text{In}}\text{H}_4$. The compensation of the annealed material is achieved mainly due to the deep acceptors with activation energies of 350 and 470 meV, which can be assigned to the excited state of Fe^{2+} and to a complex involving phosphorus antisite, respectively.

4.2 Investigation of irradiation-induced point defects in epitaxial silicon

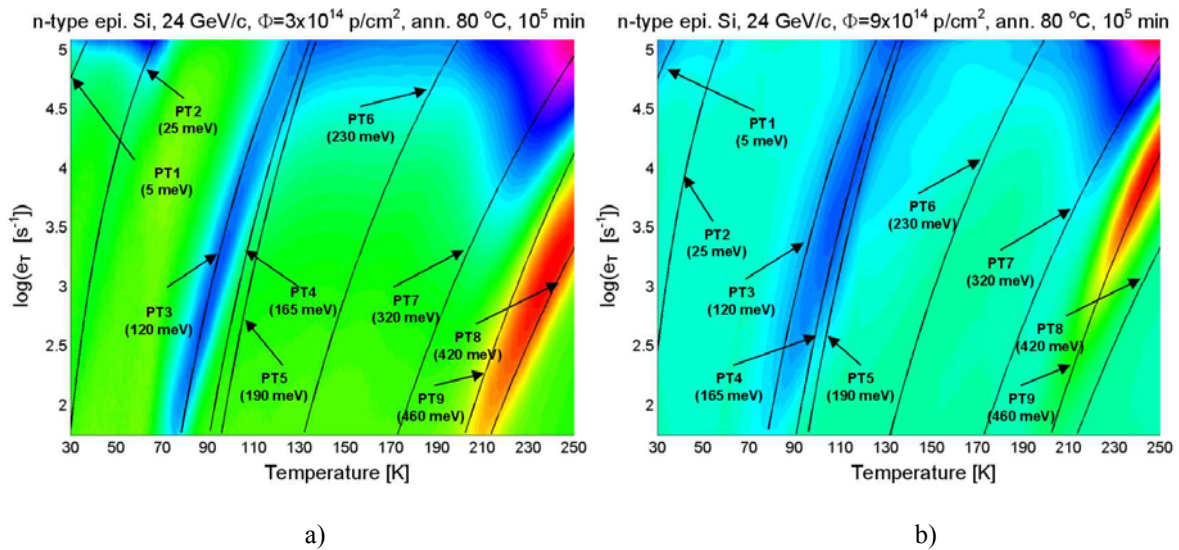


Fig. 7. Experimental spectral fringes obtained by two-dimensional correlation procedure applied to the analysis of photocurrent decays for P-doped epitaxial Si irradiated with high-energy protons and annealed at $80 \text{ }^\circ\text{C}$ for 10^5 min. (a) Proton fluence $3 \times 10^{14} \text{ cm}^{-2}$; (b) proton fluence $9 \times 10^{14} \text{ cm}^{-2}$. The solid lines illustrate the temperature dependences of emission rate for detected defect centres.

Figures 7 (a) and 7 (b) show the projections of the two-dimensional correlation spectra on the plane determined by the axes for the temperature (T) and the emission rate (e_T) for epitaxial silicon irradiated with fluences 3.0×10^{14} (sample A) and $9.0 \times 10^{14} \text{ p/cm}^2$ (sample B), respectively. It is easily seen that some broad fringes consist of several overlapping ones related to different defects. The solid lines in Figs 7 (a) and 7 (b) illustrate the temperature dependences of the emission rate for detected defect centres. As can be seen in Figs 1 (a) and 1 (b), the effect of fluence manifests itself mainly through the changes in the shape of fringes occurring in the temperature ranges of 70-130 K and 200-250 K. It should be added that the

photocurrent decays measured in the temperature range between 70-130 K were also transformed into two-dimensional spectra using the ILT algorithm and the neural network approximation was used to extract the parameters of defect centres. The higher resolution of the ILT algorithm is exemplified in Figs 8 (a) and 8 (b) showing the Laplace spectra for the samples A and B, respectively, obtained from the photocurrent decays recorded at a temperature of 100 K. The results show that each of the broad fringes, seen in Figs 7 (a) and 7 (b) between 70 and 130 K, is produced by three defect centres: PT3 (120 meV), PT4 (165 meV) and PT5 (190 meV). The spectral fringe seen for all the samples in the range of 200-250 K results from the hollow in the two-dimensional spectrum produced by negative photocurrent transients observed after switching off the source of light. These transients arise due to thermal emission of electrons from deep acceptors the occupation of which controls the electron concentration in the conduction band. According to Figs 7 (a) and 7 (b), the fringe between 200 and 250 K is composed of two overlapping fringes related to defects centres PT8 (420 meV) and PT9 (460 meV).

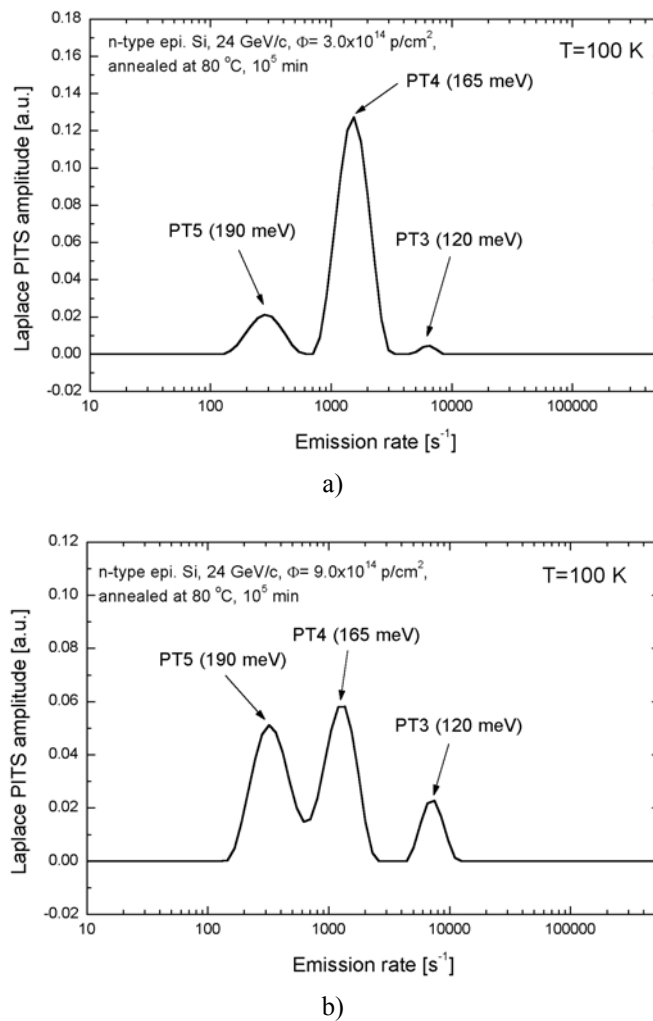


Fig. 8. PITS spectra obtained by means of inverse Laplace transform applied to the analysis of the photocurrent decay measured at 100 K for P-doped epitaxial Si irradiated with high-energy protons and annealed at 80°C for 10^5 min. (a) Proton fluence $3 \times 10^{14} \text{ cm}^{-2}$; (b) proton fluence $9 \times 10^{14} \text{ cm}^{-2}$.

The parameters of detected defect centres are summarized in Table 3. The data presented in Table 3 show that the high-energy proton irradiation and subsequent long-term annealing results in the formation of 9 defect centres with activation energies ranging from 5 to 460

meV. They include shallow donors PT1 (5 meV) and PT2 (25 meV), oxygen related complexes PT4 (165 meV), PT5 (190 meV), PT7 (320 meV) and PT9 (460 meV) as well as divacancies in different charge states PT6 (230 meV) and PT8 (420 meV). By analysing the amplitudes of the folds corresponding to the traps PT3 (120 meV), PT4 (165 meV) and PT5 (190 meV) we have found that in the sample A, irradiated with a fluence of 3.0×10^{14} p/cm², the predominant defects represent the $C_iC_s(B)^{-/0}$ complexes and the concentrations of $VO^{-/0}$ and $V_2O^{-/-}$ defects are equal to 70% and 50%, respectively, of the predominant defect concentration. On the other hand, in the sample B, irradiated with a fluence of 9.0×10^{14} p/cm², the predominant defects are $VO^{-/0}$ complexes and the concentrations of $V_2O^{-/-}$ and $C_iC_s(B)^{-/0}$ complexes are 80% and 70%, respectively, of the predominant defect concentration. On the grounds of the absolute magnitudes of the hollows related to the traps PT8 (420 meV) and PT9 (460 meV) we have estimated the effect of fluence on the concentrations of divacancies $V_2^{-/0}$ and complexes $V_2O^{-/0}$. In the material irradiated with the lower fluence the concentration of $V_2O^{-/0}$ complexes is approximately 4 times lower than that of divacancies $V_2^{-/0}$. The irradiation with the higher fluence changes the material defect structure and the concentration of $V_2O^{-/0}$ complexes is around 6 times higher compared to that of divacancies $V_2^{-/0}$.

Table 3. Parameters of defect centres detected by means of the intelligent measuring system in high-energy proton irradiated epitaxial silicon.

Label	E_T (meV)	A (s ⁻¹ K ⁻²)	σ^a (cm ²)	Tentative identification
PT1	5	3×10^2	3×10^{-19}	shallow donor, e [36,37]
PT2	25	2×10^3	2×10^{-18}	shallow donor, e [36,37]
PT3	120	5×10^5	5×10^{-16}	$C_iC_s(B)^{-/0}$, e [36,37]
PT4	165	1×10^7	1×10^{-14}	$VO^{-/0}$, e [36,37]
PT5	190	6×10^7	5×10^{-14}	$V_2O^{-/-}$ [38, 39] or $X^{-/-}$ [40], e
PT6	230	2×10^6	2×10^{-15}	$V_2^{-/-}$, e [36,37]
PT7	320	4×10^6	4×10^{-15}	$VOH^{-/0}$, e [41,42]
PT8	420	1×10^7	1×10^{-14}	$V_2^{-/0}$, e [36]
PT9	460	4×10^8	4×10^{-13}	$V_2O^{-/0}$ [38, 39] or $X^{-/0}$ [40], e

^{a)} The values of the apparent capture cross-section refer to electron traps according to the identification given in the last column.

5. CONCLUSIONS

A new approach to the characterization of defect centres in semi-insulating materials by photoinduced transient spectroscopy has been presented. It is based on the two-dimensional analysis of the photocurrent transients digitally recorded at a broad range of temperatures. The spectral analysis is carried out by two independent methods: the two-dimensional correlation procedure and the procedure based on the inverse Laplace transformation algorithm. The former method, employing the Dirac's delta function with a shift at the two time points, is of lower resolution. The folds on the spectral surface are usually broad due to superposition of the thermal emission processes of charge carriers from several defect centres. However, it enables a qualitative image of the material defect structure to be quickly obtained. The latter method, relying on fitting of the photocurrent decays with multi-exponential functions by means of the CONTIN program, is of higher resolution. It is however more sensitive to the noise component in the photocurrent decays, which leads to some artefacts occurring in the spectra. The new approach has been implemented in the intelligent measuring system enabling the computational intelligence to be used for determination of the trap parameters of the grounds of the spectral fringes obtained as a result of the two-dimensional correlation procedure or inverse Laplace transform. The basic tool used for extraction of the defect

centres parameters from the photocurrent decays is the neural network in the form of two-layered perceptron whose inputs are the arguments of the spectral surface. The activation function of hidden neuron is represented by the weighted sum of two sigmoid functions. So, each hidden neuron can model the lateral surface of the two-dimensional spectrum and when added together, they created the fold that matches the experimental fold corresponding to a specific defect centre. The parameters of these centres, such as activation energy and apparent capture cross section are directly obtained using an optimization process as the weight coefficients of the hidden neurons. The potentialities of the intelligent measuring system are exemplified by studies of electrically active defects in SI InP and in radiation defects in high-resistivity epitaxial silicon. The comparison of the defect structure of SI InP, obtained by doping with Fe in the LEC process, and that of undoped SI InP, obtained through the high-temperature annealing of the low-resistivity material in pure phosphorus ambience, is presented. In the case of the proton irradiated epitaxial silicon, the changes in the defect structure induced by the increase of fluence from 3.0×10^{14} to 9.0×10^{14} p/cm² are shown.

ACKNOWLEDGEMENTS

The work described in this paper was partially supported by the Polish Ministry of Scientific Research and Information Technology under Grant 4 T11B 068 24.

REFERENCES

1. Hirt G., Hofmann D., Mosel F., Schafer N., Muller G.: *Compensation mechanisms in normally undoped semi-insulating InP and comparison with undoped InP Grown under stoichiometry control*, J. Electronic Mat., vol. 20, no. 12, 1991, pp. 1065-1068.
2. Dreszer P., Chen W. M., Seendripu K., Wolk J. A., Walukiwicz W., Liang B. W., Tu C. W., Weber E. R.: *Phosphorus antisite defects in low-temperature InP*, Phys. Rev. B, vol. 47, no. 7, 1993, pp. 4111- 4114.
3. Fang Z.-Q., Look D. C., Uchida M., Kainosho K., Oda O.: *Deep Centers in Undoped Semi-Insulating InP*, J. Electronic Mat., vol. 27, no. 10, 1998, pp. L68-L71.
4. Lang D. V.: *Deep-level transient spectroscopy: A new method to characterize traps in semiconductors*, J. Appl. Phys., vol. 45, no. 7, 1974, pp. 3023-3032.
5. Kuriyama K., Tomizawa K., Kashiwakura M., Yokoyama K.: *Characterization of deep level defects in thermally annealed Fe-doped semi-insulating InP by thermally stimulated current spectroscopy*, J. Appl. Phys., vol. 76, no. 6, 1994, pp. 3552-3555.
6. Marrakchi G., Cherkaoui K., Karoui A., Hirt G., Muller G.: *Traps in undoped semi-insulating InP obtained by high temperature annealing*, J. Appl. Phys., vol. 79, no.9, 1996, pp. 6947-6950.
7. Zhao Y., Dong H. W., Jiao J., Zhao J., Lin L.: *Fe-Diffusion-Induced Defects in InP Annealed in Iron Phosphide Ambient*, Jpn. J. Appl. Phys., vol. 41, no. 4A, 2002, pp. 1929-1931.
8. Hirt G., Mono T., Muller G.: *Preparation and characterization of semi-insulating 2''InP wafers having a low Fe content by wafer annealing*, Mat. Sci. Eng. B26, 1994, pp. 91-100.
9. Hurtes C., Boulou M., Mitonneau A., and Bois D.: *Deep-level spectroscopy in high-resistivity materials*, Appl. Phys. Lett., vol. 32, no. 12, 1978, pp. 821-823.
10. Yoshie O., Kamihara M.: *Photo-Induced Current Transient Spectroscopy in High-Resistivity Bulk Material. II. Influence of Non-Exponential Transient on Determination of Deep Trap Parameters*, Jpn. J. Appl. Phys., vol. 22, no. 4, 1983, pp. 629-635.
11. Abele J.C., Kremer R.E., Blakemore J. S.: *Transient photoconductivity measurements in semi-insulating GaAs. II. A digital approach*, J. App. Phys., vol. 62, no. 6, 1987, pp. 2432- 2438.
12. Longeaud C., Kleider J.P., Kamiński P., Kozłowski R., Pawłowski M., Ćwirko J.: *Investigation of defect levels in semi-insulating materials by modulated and transient photocurrent: comparison of methods*, Semicond. Sci. Technol., vol. 14, 1999, pp. 747-756.
13. Kamiński P., Kozłowski R.: *High-resolution transient spectroscopy as a new tool for quality assessment of semi-insulating GaAs*, Materials Science and Engineering B, vol. 91-92, 2002, pp. 398-402.
14. Kozłowski R., Kamiński P., Nossarzewska-Orłowska E.: *High-resolution photoinduced spectroscopy as a new characterisation tool for defect engineering of irradiated silicon*, Proceedings of First ENDEASD Workshop, Santorini, Greece, 1999, pp. 186-195.

15. Pawłowski M.: *Extraction of deep trap parameters from photocurrent transients by two-dimensional spectral analysis*, Sol. State Electron., vol. 46, 2002, pp. 1879-1885.
16. Kaminski P., Pawłowski M., Cwirko R., Palczewska M., Kozłowski R.: *Investigation of deep-level defects in semi-insulating GaAs and InP by analysis of photo-induced current transient*, Mat. Sci. Eng. B, vol. 42, 1996, pp. 213-216.
17. Istratov A. A.: *The resolution limit of traditional correlation functions for deep level transient spectroscopy*, Rev. Sci. Instrum., vol. 68, no. 10, 1997, pp. 3861-3865.
18. Look D.C.: *The electrical and photoelectronic properties of semi-insulating GaAs*. In: Willardson R.K., Beer A.C., editors. Semiconductors and semimetals, vol. 19. New York: Academic Press, 1983.
19. Pawłowski M., Kaminski P., Kozłowski R., Miczuga M.: *Laplace transform photoinduced transient spectroscopy: new powerful tool for defect characterisation in semi-insulating materials*, SPIE Proceedings, vol. 5136, 2003, pp. 59-65.
20. Dobaczewski L., Kaczor P., Hawkins I. D., Peaker A. R.: *Laplace transform deep-level transient spectroscopic studies of defects in semiconductors*, J. Appl. Phys., vol. 76, no. 1, 1994, pp. 194-198.
21. Istratov A. A., Vyvenko O. F.: *Exponential analysis in physical phenomena*, Rev. Sc. Inst., vol. 70, no. 2, 1999, pp. 1233-1257.
22. Provencher S. W.: *A constrained regularization method for inverting data represented by linear algebraic or integral equations*, Comp. Phys. Comm., vol. 27, 1982, pp. 213-227.
23. Provencher S. W.: *CONTIN: A general purpose program for inverting noisy linear algebraic and integral equations*, Comp. Phys. Comm., vol. 27, 1982, pp. 229-242.
24. Jankowski S., Wierzbowski M., Kaminski P., Pawłowski M.: *Implementation of neural network method to investigation of defect centers in semi-insulating materials*, International Journal of Modern Physics B, vol. 16, no. 28 & 29, 2002, pp. 4449-4454.
25. Bishop M. C.: *Neural Networks for Pattern Recognition*, Clarendon Press, Oxford, 1995.
26. Shmidt: *Handbook Series on Semiconductor Parameters*, vol. 1, M. Levinshtein, S. Rumyantsev, M. Shur, ed., World Scientific, London, 1996
27. Mayer K. M., Makita Y., Yamada A., Shibata H., Beye A. C., Shimada J.: *Characterization of processing-induced defects in high-purity InP by photoluminescence*, J. Appl. Phys., vol. 72, no. 3, 1992, pp. 1080-1085.
28. Surma B., Wnuk A., Dubecky F., Piersa M., Strzelecka S., Hruban A., in *Proceedings of SIMC-XII 2002, Smolenice, Slovak Republic*, 2003.
29. Kang J., Matsumoto F., Fukuda T.: *Photoluminescence of undoped bulk InP grown by the liquid-encapsulated vertical Bridgman technique*, J. Appl. Phys., vol. 81, no. 20, 1997, pp. 905-909.
30. Shan Y. Y., Deng A. H., Ling C. C., Fung S., Ling C. D., Zhao Y. W., Sun T. N., Sun F.: *Positron-annihilation study of compensation defects in InP*, J. Appl. Phys., vol. 91, no. 4, 2002, pp. 1998-2001.
31. Polity A. and Engelbrecht T.: *Defects in electron-irradiated InP studied by positron lifetime spectroscopy*, Phys. Rev. B, vol. 55, no. 16, 1997, pp. 10 480-10 486.
32. Nicholas D. J., Allsopp D., Hamilton B., Allsopp A. R., Bass S. J., J. Cryst. Growth, vol. 68, 1984, pp. 326-333.
33. Wolf T., Drews D., Scheffler H., Bimberg D., Mosel F., Kipfer P., Muller G.: *Identification of deep levels in liquid-encapsulation Czochralski-grown Fe- and Zn-doped InP: A proof of the nonexistence of a Fe^{4+}/Fe^{3+} donor level*, J. Appl. Phys., vol. 73, no. 10, 1993, pp. 226-232.
34. Kaminski P., Thomas H.: *Characterization of deep traps in semi-insulating GaAs and InP by photoinduced transient spectroscopy (PITS)*, Acta Phys. Pol., vol. A77, no. 1, 1990, pp. 87-90.
35. Fornari R., Brinciotti A., Gombia E., Mosca R., Sentiri A., Mat. Sc. Eng. B, vol. 28, 1994, pp. 95-100.
36. Kaminski P., Kozłowski R., Nossarzewska-Orłowska E.: *Formation of electrically active defects in neutron irradiated silicon*, Nucl. Instr. and Meth. B, vol. 186, 2002, pp. 152-156.
37. Kaminski P., Kozłowski R., Jelenski A., Mchedlidze T., Suezawa M.: *High-resolution photoinduced transient spectroscopy of electrically active iron-related defects in electron irradiated high-resolution silicon*, Jap. J. Appl. Phys. vol. 42, 2003, pp. 5415-5419.
38. Mikelsen M., et al.: *Annealing behaviour of defects in irradiated MCZ- and DOFZ-Si detector materials*, presented on the 4th RD50 Workshop, 5-7 May 2004, CERN, Geneva, Switzerland.
39. Alfieri G., Monakhov E. V., Avset B. S., Svensson B. G.: *Evidence for identification of the divacancy-oxygen center in Si*, Phys. Rev. B, vol. 68, 2003, pp. 233202-233205.
40. I. Pintilie et al.: *The X defect in Epi/Cz silicon diodes after high doses of Co^{60} - γ irradiation*, presented on the 5th RD50 Workshop, 14-16 October 2004, Florence, Italy.
41. Da Via C., Watts S. J.: *New results for a novel oxygenated silicon material*, Nucl. Instr. and Meth. B, vol. 186, 2002, pp. 111-115.
42. Andersen O., Dobaczewski L., Peaker A. R., Nielsen Bonde K., Hourahine B., Jones R., Briddon P. R., Öberg S.: *Piezospectroscopic analysis of the hydrogen-carbon complexes in silicon*, Physica B: Physics of Condensed Matter, vol. 308, 2001, pp. 139-142.

INTELIĞENTNY SYSTEM POMIAROWY DO BADANIA CENTRÓW DEFECTOWYCH W MATERIAŁACH PÓLIZOLUJĄCYCH METODĄ NIESTACJONARNEJ SPEKTROSKOPII FOTOPRĄDOWEJ

Streszczenie

Przedstawiono inteligentny system pomiarowy dedykowany do charakteryzacji centrów defektowych w materiałach półizolujących. Działanie systemu polega na rejestracji relaksacyjnych przebiegów fotoprądu w szerokim zakresie temperatur oraz realizacji dwuwymiarowej analizy temperaturowych zmian stałych czasowych tych przebiegów. Analiza widmowa przeprowadzana jest za pomocą dwóch niezależnych metod: dwuwymiarowej procedury korelacyjnej i procedury wykorzystującej odwrotną transformatę Laplace'a. Parametry centrów defektowych wyznaczane są za pomocą sieci neuronowej, która złożona jest z dwóch neuronów w postaci dwuwymiarowych funkcji tangensa hiperbolicznego i realizuje morfologiczne dopasowanie funkcji aproksymującej do kształtu fałdy na powierzchni widmowej. Wartości parametrów centrów defektowych otrzymywane są jako wartości parametrów aproksymatora po procesie dopasowania. Przedstawiono przykłady zastosowania systemu do badania centrów kompensujących w półizolującym InP oraz centrów radiacyjnych w krzemowych, wysokorezystywnych warstwach epitaksjalnych napromieniowanych protonami o dużej energii. Porównano strukturę defektową SI InP domieszkowanego żelazem w procesie monokryształizacji oraz strukturę defektową SI InP, którego półizolujące właściwości otrzymano w wyniku długotrwałej obróbki termicznej w atmosferze par fosforu. W krzemowych warstwach epitaksjalnych określono zmiany struktury defektowej w funkcji dawki protonów.